Laser and Particle Beams (2015), *33*, 379–386.

doi:10.1017/S0263034615000452

Efficiency of ablative plasma energy transfer into a massive aluminum target using different atomic number ablators

A. KASPERCZUK,[1] T. PISARCZYK,[1] T. CHODUKOWSKI,[1] Z. KALINOWSKA,[1] W. STEPNIEWSKI,[1] K. JACH,[2] R. SWIERCZYNSKI,[2] O. RENNER,[3] M. SMID,[3] J. ULLSCHMIED,[3,4] J. CIKHARDT,[5] D. KLIR,[5] P. KUBES,[5] K. REZAC,[5] E. KROUSKY,[4] M. PFEIFER,[4] AND J. SKALA[4]

[1]Institute of Plasma Physics and Laser Microfusion, Warsaw, Poland
[2]Institute of Optoelectronics, Military University of Technology, Warsaw, Poland
[3]Institute of Physics ASCR, v.v.i., Prague, Czech Republic
[4]Institute of Plasma Physics ASCR, v.v.i., Prague, Czech Republic
[5]Czech Technical University in Prague, FEE, Prague, Czech Republic

(RECEIVED 13 February 2015; ACCEPTED 28 March 2015)

Abstract

This paper aims at investigation of efficiency of an ablative plasma energy transfer into a massive aluminum target using different atomic number ablators. For this reason, several target materials representing a wide range of atomic numbers ($Z = 3.5$–73) were used. The experiment was carried out at the iodine Prague Asterix Laser System. The laser provided a 250 ps pulse with energy of 130 J at the third harmonic frequency ($\lambda_3 = 0.438$ μm). To study the plasma stream configurations a four-frame X-ray pinhole camera was used. The electron temperature of the plasma in the near-surface target region was measured by means of an X-ray spectroscopy. The efficiency of the plasma energy transport to the target was determined via the crater volume measurement using the crater replica technique. The experimental results were compared with two-dimensional numerical simulations where the plasma dynamics was based on the one-fluid, two temperature model, including radiation transport in diffusive approximation and ionization kinetics. It was shown that the plasma expansion geometry plays an important role in the ablative plasma energy transfer into the target.

Keywords: Ablator atomic number; Crater volume; Laser energy transfer; Plasma ablative pressure; Plasma expansion geometry; Plasma temperature

1. INTRODUCTION

Inertial confinement fusion (ICF) is an approach to fusion that relies on the inertia of the fuel mass to achieve confinement. At present, studies in the field of ICF develop in the framework of two ignition concepts, namely, hydrodynamic spark ignition (including ignition by a focused shock wave) and fast ignition (Lindl, 1995; Ribeyre *et al.*, 2009; Gus'kov, 2013). These concepts are based on different methods for the coordination of the processes of plasma compression and heating and different methods for igniter formation.

This paper studies the ablative plasma energy transfer into a massive aluminum target in dependence on atomic number of the ablator. We will only consider the configuration with the target directly irradiated by the laser beam (the so-called direct compression). Being absorbed in the target, the driver radiation heats and evaporates the target material. The hot plasma generated on the outer surface of the target (ablator) expands against the incident driver radiation. Under the action of the pressure of the evaporated part of the target (the so-called ablation pressure), the shock wave is generated in the inner part of the target. A key component of this target is the outer ablator layer responsible for the absorption of the laser radiation and formation of the ablation pressure. The ablator consists of low atomic number Z materials (e.g. DT-ice, various plastics, beryllium, etc.) to minimize energy losses caused by the plasma thermal emission.

The growth of the thermal emission with the increasing atomic number of the ablator leads to a decrease of the ablative plasma pressure. The degree of the plasma pressure reduction with the growing Z is an important issue. Our previous experiments, carried out at the Prague Asterix Laser System (PALS) iodine laser facility, indicated that the inner plasma pressure decreases with the growing Z (Kasperczuk *et al.*, 2013; 2014). This research was performed using the

Address correspondence and reprint requests to: T. Pisarczyk, Institute of Plasma Physics and Laser Microfusion, Warsaw, Poland. E-mail: tadeusz.pisarczyk@ifpilm.pl

massive targets of Al ($Z = 13$), Cu (29), Ag (47), and Ta (73) with a cylindrical CH (3.5) insert of diameter $\Phi_{in} = 200$ μm. In context with the results obtained, a question arose what is an efficiency of the ablative plasma pressure transfer into the target for ablators with different atomic number. To clarify this problem, we realized further experiments using the massive Al targets covered by different thin layers (ablators) of CH, Mg, Cu, Ag, and Ta.

The ablative plasma energy transfer into the target is mainly realized by the shock wave propagating into the target just after the laser pulse termination. However, conditions of the shock wave generation largely depend on the ablator material. The essential information on the energy transfer efficiency for ablators with various atomic numbers can be obtained by measuring the following parameters:

- geometry of the ablative plasma expansion,
- electron temperature of the Al plasma for different ablators used, and
- volume of a crater produced by the shock wave propagating into the massive Al target.

Consequently, these issues were studied in the investigation reported.

2. EXPERIMENTAL SETUP AND CONDITIONS

The experiment was carried out with the use of the PALS laser facility. For plasma generation we used a laser beam of diameter 290 mm, which was focused by means of an aspherical lens with a focal length of 600 mm optimized for the third harmonic of the laser radiation used ($\lambda = 0.438$ μm). The targets were irradiated using the laser energy $E_L = 130$ J, focal spot radius $R_L = 300$ μm (the focal point being located inside the target), and the pulse duration of 250 ps [full width at half maximum (FWHM)].

To study the plasma stream formation, a four-frame pinhole X-ray imaging system was used. The camera with a pinhole diameter of 80 μm registered soft X-ray plasma radiation in the range of 10–1000 eV. The exposure time was below 2 ns.

The electron temperature of the plasma in the near-surface target region was measured by means of an X-ray spectroscopy. The efficiency of the plasma energy transport to the target was determined on the basis of the crater volume measurement using the crater replica technique.

3. DETERMINATION OF THE ABLATOR THICKNESSES

Thin layers of CH, Mg, Cu, Ag, and Ta were used as ablators. Being applied as the massive target, aluminum could not meet a criterion for the ablator, because in such case the electron temperature of Al plasma would be measured during the laser pulse action, not as in the other cases after the laser pulse end. Therefore aluminum was substituted by magnesium with $Z = 12$.

In turn, it was very important to determine proper thicknesses of ablators which should be completely vaporized by the laser pulse action to assure in each the case the same conditions for the energy transfer into the massive Al target. However, an estimation of their thicknesses caused some problems. The scaling of mass ablation rate with laser intensity taken from the literature requires exact information about the laser beam intensity on the target. In the case of the PALS laser, determination of the intensity distribution on the target makes a great problem. The gas (iodine) PALS laser tends to generate a central depression in the transverse beam cross-section. Thus, the target irradiation geometry in the PALS experiments is annular-like. So, the ablator thickness should be matched to varying intensity of the laser beam on the target.

Working on the assumption that the Al plasma expansion should occur after the ablator evaporation, determination of time relations between the laser pulse and the Al plasma expansion for the each ablator used turned out to be an essential question. For this reason the X-ray camera was employed. The plasma stream configurations recorded by it at defined instants supplied expected information on a delay of the Al plasma expansion respecting the laser pulse.

A choice of the ablator thicknesses started from CH foil, the optimum thickness of which proved to be 500 nm. Sample results of our tests consisting of three sequences of X-ray images are shown in Figure 1. Here CH means a CH massive target, CH(Al) – an Al massive target covered by a 500 nm-thick CH foil and Al – an Al massive target. For the time of about 0 ns, which corresponds to the period of the laser action (bearing in mind the X-ray camera exposure time), there is no difference between the images taken at CH and CH(Al) targets, whereas in the case of the Al target the intensity of the plasma X-ray radiation is considerably higher. At 3 ns later, the images for the CH(Al) and Al targets become very similar each to other, while that for the CH target is still characterized by a very low intensity. It means that 2–3 ns after the laser pulse termination, the CH foil is completely vaporized. At later time, the Al plasma appears which shines very intensively.

Having correctly determined the CH layer thickness, the thicknesses of the other ablators required to be correctly chosen. The above-mentioned annular-like geometry of the target irradiation plays a decisive role in the plasma jet formation. This plasma jet is produced by the collision of plasma flows converging on the axis. The detailed ablative plasma expansion geometries recorded for different massive targets by means of a three-frame interferometric system were presented in our earlier papers (e.g., Kasperczuk *et al.*, 2009). They proved that the CH and Al plasma streams differ essentially from those launched from heavier targets. The light plasmas such as CH and Al have a tendency to a hemispherical expansion, whereas the heavier ones expanding rather axially create the plasma jets with high plasma density in the axial region.

https://doi.org/10.1017/S0263034615000452 Published online by Cambridge University Press

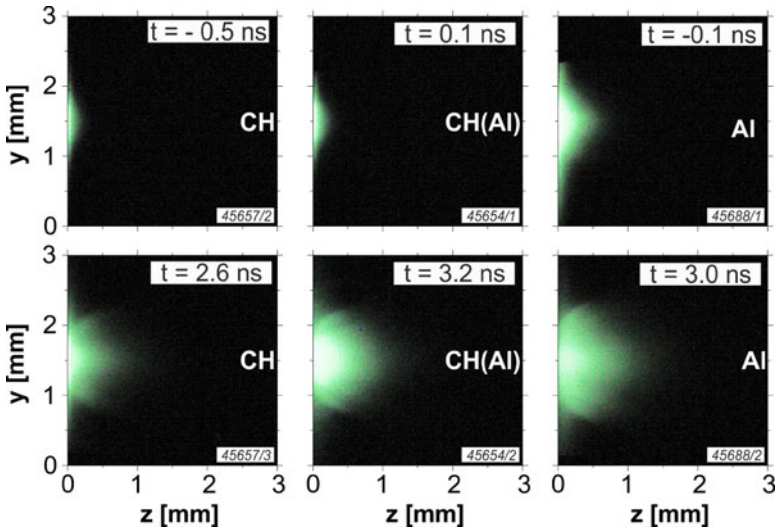

Fig. 1. Three sequences of X-ray images visualizing the plasma launched on CH massive target, Al massive target covered by 500-nm-thick CH foil, and Al massive target.

The thicknesses of other ablators were established indirectly taking advantage of the above information. Starting from the CH layer thickness they were somewhat arbitrary reduced respectively with the growing Z of the ablator. However, to be certain of the correct choice of ablator thicknesses the series of X-ray plasma images for all ablators at time of ~3 ns was recorded (see Fig. 2). The jet-like form of the heavy plasma streams seen at this instant allowed us to conclude that the Al plasma expansion starts at least 1–2 ns after the laser pulse end. The early Al plasma expansion, especially still during the laser pulse action, should result in a disappearance of the plasma jet configuration which is not observed.

The established thicknesses of all ablators used are shown in Table 1.

4. MEASUREMENT OF ELECTRON TEMPERATURE OF THE AL PLASMA

The information on electron temperature of the plasma created on the surface of bare or coated Al targets was provided by X-ray spectroscopy. The Al K-shell self-emission spectra were recorded using the imaging X-ray spectrometer equipped with the mica (006) crystal spherically bent to a radius of 150 mm. The detector was placed at intersection of the central ray with the Rowland circle (Renner *et al.*, 2004) thus providing the maximum spectral resolution close to the intrinsic value of $\lambda/\Delta\lambda \approx 11{,}900$ following from the dynamical theory of X-ray diffraction on the bent mica crystal. Using the source-to-crystal and crystal-to detector distances of 198.6 and 138.1 mm, respectively, the spectrometer covered the spectral range of approximately 6.0–6.2 Å, including emission lines of hydrogenic Al Lyβ and transitions δ–η in He-like Al. The one-dimensional (1D) spatial resolution was obtained with demagnification of 0.7 in the direction perpendicular to the vertical dispersion plane. The spectra were observed at an angle of $14.5° \pm 0.2°$ with respect to the surface of irradiated targets. The spatially resolved, time-integrated spectra were recorded on the X-ray film Kodak Industrex AA400. The spectral records were digitized and transformed to the intensity and the wavelength scale using the characteristic curve of the film and the ray-traced dispersion relation.

An example of the reconstructed experimental data together with the best-fit synthetic spectrum is represented in Figure 3. The emission from the surface of the bare Al target contains dominant resonance Lyβ line ($3p\ ^2P_{3/2,1/2} \rightarrow 1s\ ^2S_{1/2}$, 6.053 Å) of hydrogenic Al and Heϵ ($1s6p\ ^1P_1 \rightarrow$

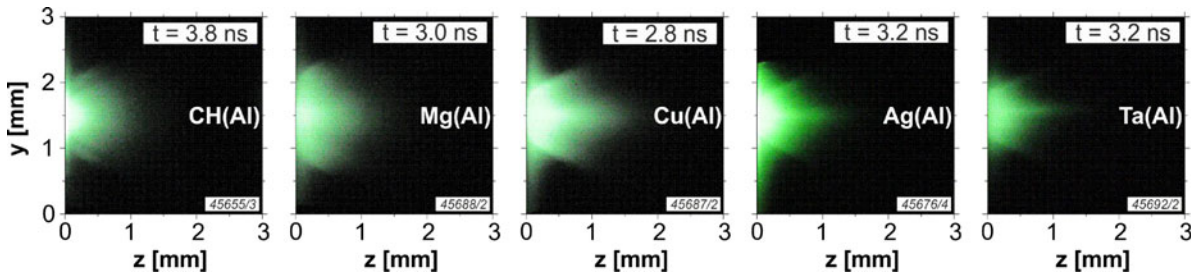

Fig. 2. X-ray plasma images for all ablators used at instant of ~3 ns.

https://doi.org/10.1017/S0263034615000452 Published online by Cambridge University Press

Table 1. *Type, atomic number (Z), and thickness of ablators in nm*

Ablator	CH	Mg	Cu	Ag	Ta
Z	3.5	12	29	47	73
Thickness	500	300	210	170	100

$1s^2\ ^1S_0$, 6.103 Å) and Heδ ($1s5p\ ^1P_1 \rightarrow 1s^2\ ^1S_0$, 6.176 Å) transitions of He-like Al ions. The comparison of the measured spectral profiles with theoretical spectra provided information on the plasma temperature and density.

The details of the fitting procedure can be found in paper (Šmíd *et al.*, 2013), here we describe only its basic principles. The experimental data evaluation was based on Prism SPECT package (MacFarlane *et al.*, 2007) for synthesis of X-ray spectra. The model used depends on three parameters, namely the plasma temperature T, mass density ρ, and size L, thus the fitting procedure represented a three-step process. First, the density was inferred from the broadened profile of the Heδ line. The width of this profile is dependent on ρ and in the same time, the Heδ emission is characterized by a low optical thickness, thus the role of the plasma size L is marginal. Second, having the density fixed, the effective plasma size was estimated by fitting the width of the Lyβ, as this line with strong reabsorption undergoes significant opacity broadening. The found plasma densities varied within $\rho = 0.015$–$0.030\ \mathrm{g/cm^3}$ and the effective sizes were in the range of $L = 20$–$100\ \mu\mathrm{m}$. Finally, the plasma temperature was estimated using the ratio of Lyβ and Heδ lines. This ratio is strongly dependent on the temperature since these transitions originate in different ionization states.

The spectra fitting was rather straightforward for the pure Al target and for the targets with CH and Mg ablators, since the diagnostic Al transitions were not overlapped by spectral lines emitted from low-Z ablators. When using Ta and Cu ablators, the presence of their transitions within the diagnostic range of 6.0–6.2 Å complicated the precise spectra evaluation but still the plasma temperature could be determined without principal difficulties (see Fig. 4).

The final results are depicted in Figure 5. The diagram shows the electron temperature of the Al plasma produced using ablators with different Z. Up to $Z = 47$, the temperature drops markedly with the increasing Z. This proves that the ablative plasma cooling is very effective in this range of Z. However, for $Z > 47$ the temperature stagnation is observed. It suggests that for ablators with large Z the energy losses are roughly kept on the same level.

In the above diagram, the electron temperature of the Al plasma for the bare Al target is marked, too. Based on this, the energy losses corresponding to individual ablators can be estimated. Obviously for the Al target coated with the CH layer, the temperature is only slightly smaller than that observed using the bare Al target.

5. DETERMINATION OF VOLUMES OF CRATERS PRODUCED IN THE MASSIVE AL TARGET

The efficiency of the plasma energy transfer to a solid part of the target was determined via the crater volume measurement using the crater replica technique. To obtain information about the crater characteristics, the crater replicas were made of cellulose acetate. To find the crater volume, profiles of the crater replica in chosen cross-sections were digitized and used for calculations.

To improve statistics of the crater volume measurements, for each kind of the ablator a few laser shots were done. The crater volumes plotted in dependence on the ablator atomic number are presented in Figure 6. We underline the most important finding coming from this dependence. Despite the fact that the CH plasma exhibits the highest pressure, the corresponding crater volume is minimal in comparison with other cases. A maximum value of the crater volume is reached for the Cu ablator. With further growing Z, the crater volume decreases again until

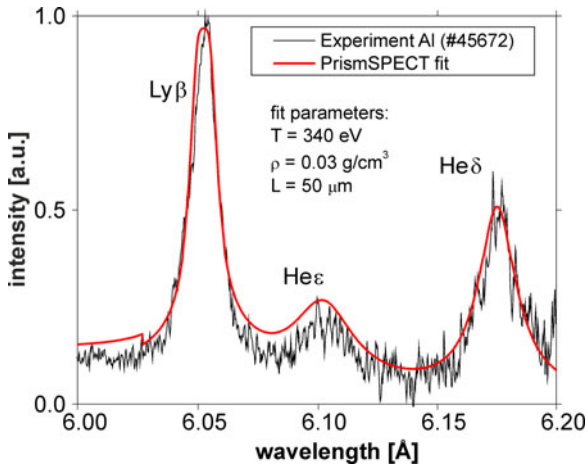

Fig. 3. Comparison of the experimental spectrum emitted from the pure Al target with the best-fit data synthesized by PrismSPEC code.

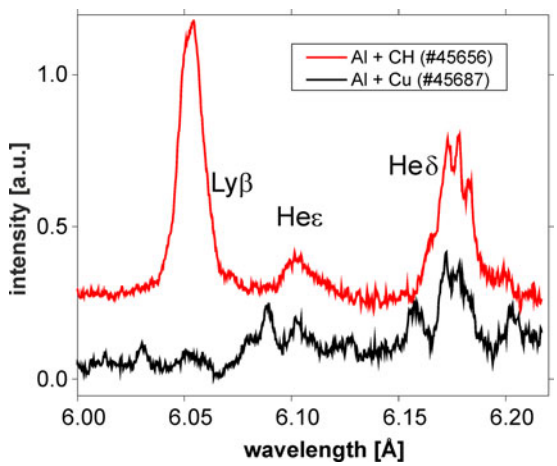

Fig. 4. Sample spectra obtained for light (CH) and heavy (Cu) ablators.

https://doi.org/10.1017/S0263034615000452 Published online by Cambridge University Press

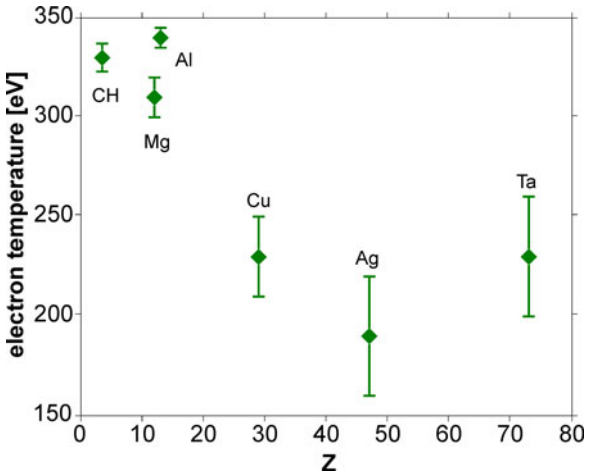

Fig. 5. Electron temperature of the Al plasma produced on targets using ablators with different atomic number *Z*.

approximately $Z = 47$. Further increase in Z induces a certain growth of the crater volume.

The dependence of the crater volume on the atomic number is rather complex and suggests that the ablative plasma energy transfer into the massive aluminum target depends on competitive factors, the activity of which changes with the increasing *Z*. This phenomenon will be discussed in the next sections.

6. NUMERICAL SIMULATIONS

Although the above-presented experimental results confirm a strong influence of the ablator atomic number on the laser energy transfer into the massive target, physical aspects of this process are not clear. To shed more light on underlying mechanisms, numerical simulations of the laser beam action directly on the CH, Al, Cu, Ag, and Ta ablators covering the Al massive target were performed. The thicknesses of ablators were the same as those used in the experiment.

The numerical simulation has been carried out by means of the two-dimensional (2D) hydrodynamic code KAROL

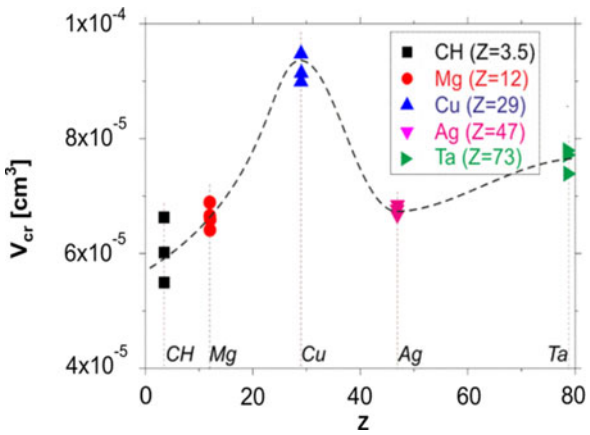

Fig. 6. Dependence of the crater volume on the ablator atomic number.

employing the meshless – "free point" method (Jach *et al.*, 2001). The computations started from the room temperature (a so-called "cold start"). Dynamics in the solid region was described by viscous-plastic equations with the Johnson–-Cook model of material strength. The processes of melting and vaporization were taken into account (Marczak *et al.*, 2010). Dynamics of plasma was based on a one-fluid, two-temperature model with radiation transport in diffusive approximation and with ionization kinetics. Laser absorption was described by the combination of the empirical formula and the inverse bremsstrahlung model. Properties of the material and plasma are described by the wide range equation of state (Gus'kov *et al.*, 1997).

To provide a proper description of the processes of the target material ablation and plasma expansion, the laser pulse parameters should be consistent with experimental parameters described in the previous section. However, as the thickness of ablators used in the experiment was very small, a very fine grid should be applied in simulations which results in very time-consuming calculations. To avoid this problem, the focal spot radius (R_L) of the laser beam striking the target was reduced from 300 to 50 μm while keeping the radiation intensity on the level of 10^{14} W/cm^2. We anticipate that this simplification did not introduced essential changes in the course of the processes under investigation.

The temporal profile of the radiation intensity $I(t)$ was described by an isosceles trapezoid with 0.442 ns in the base and FWHM duration of 0.25 ns. The intensity profile on the target had a super-Gaussian distribution $I(r) \sim \exp[-(r/R_L)^n]$, where $n = 6$.

The electron temperature of the plasma was taken as an efficiency indicator of the laser energy transfer into the plasma. Selected results of calculations are presented in Figures 7 and 8 showing spatial distribution sequences of the plasma electron temperature during the laser pulse action for different ablators. In addition to information about the plasma temperature, these figures also visualize the geometry of the plasma expansion. Large differences in the plasma expansion character between the light plasmas (produced from CH and Al ablators; Fig. 7) and the heavy ones (Cu, Ag, and Ta; Fig. 8) are obvious. While the light plasmas display a tendency to 2D expansion (r,z), cf. the case of the CH plasma, the heavy plasma expansion has 1D character (z). This is caused by differences in the plasma temperature in both cases. The efficiency of the energy transfer to the plasma is governed by processes of the laser absorption and by the plasma energy losses due to ionization and self-radiation. The calculations show that the maximum values of the ionic charge averaged over the different types of ions achieved at time of 0.2 ns amount to 3.5, 11.3, 13.5, 14.3, and 17.5 for CH, Al, Cu, Ag, and Ta ablators, respectively. In the case of CH and Al plasmas, the fraction of the lost energy does not exceed a few percent of the laser energy absorbed in the plasma. This means that the laser radiation absorption dominates the energy losses during the whole period of the

https://doi.org/10.1017/S0263034615000452 Published online by Cambridge University Press

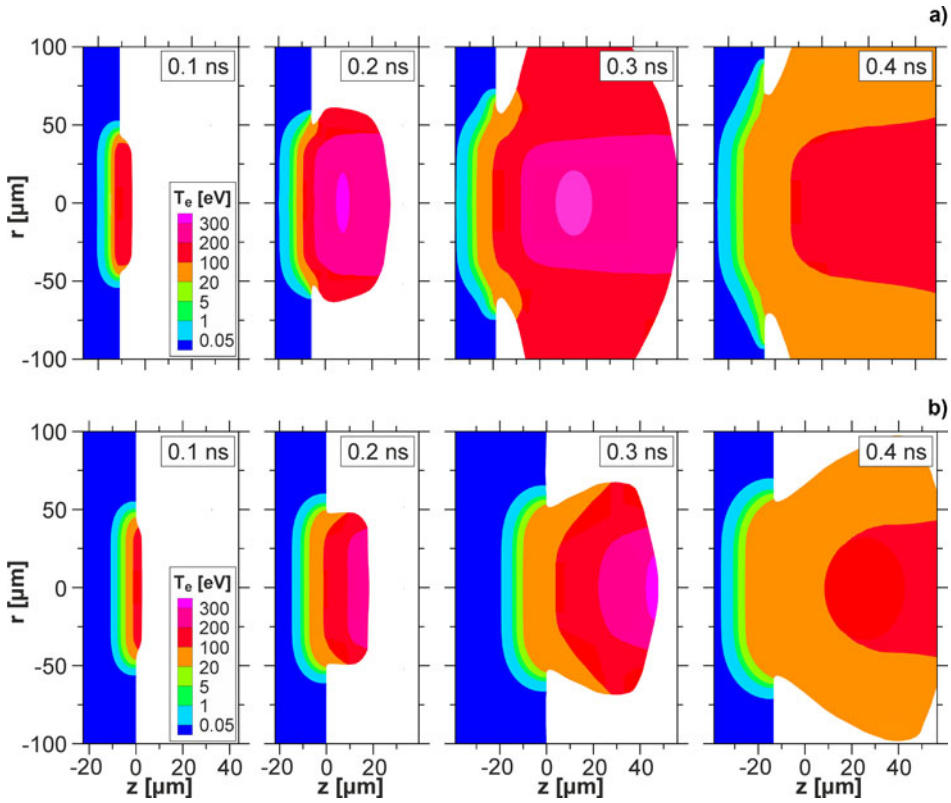

Fig. 7. Spatial distribution sequences of the plasma electron temperature during the laser pulse action simulated for different ablators: a – CH and b – Al.

laser action and the plasma can reach a high temperature. The high inner pressure of the CH and Al plasmas induces their radial expansion and the hemispherical plasma configuration is observed. In contrast, in the case of heavy plasmas the inner energy drops rapidly due to the plasma self-radiation thus restricting the radial expansion. Consequently, the plasma expands mainly axially and its front surface is planar.

Further calculations concern the Al plasma neighboring the plasmas produced from the ablators. In Figure 9, the changes of the maximal electron temperature of the Al plasma in the period of the laser action are plotted for all above-discussed ablators. We note that in the case of light ablators (CH and Al), the Al plasma temperature grows monotonically up to time of 0.3 ns, reaching the value of about 330 eV. Later on, this temperature decreases with the decreasing laser beam intensity. In the case of heavy ablators, the Al plasma reaches its maximum electron temperature already after 0.15 ns. In the period of 0.15–0.3 ns, the temperatures of Al plasmas for the Cu and Ta ablators are stabilized on the level of 220 eV. Presumably the period of stabile temperatures corresponds to the equilibrium between the processes of the laser radiation absorption and the energy loss in the plasma as a whole. However, in the case of the Ag ablator the maximal electron temperature of the Al plasma reaches only 200 eV. Later on, time a small decline in the temperature (by 20 eV) is observed. It can testify to predominance of the energy loss over the laser radiation absorption.

The above differences in the Al plasma temperatures are not traceable by this numerical modeling. The processes of heating and cooling the plasma are very complex since several competitive factors, for example, a degree of plasma ionization, plasma thermal emission, time of electron–ion relaxation, electron thermal conductivity, and electron pressure, influence the final values. To explain a role of each of them a series of simulations is required excluding successively individual factors.

7. DISCUSSION OF THE RESULTS AND CONCLUSIONS

This paper contributes to investigation of the efficiency of the ablative plasma energy transfer into massive aluminum targets using different atomic number ablators. As an indicator of this efficiency, the crater volumes produced in the massive Al targets were employed.

The crater is formed as a result of phase transformation (melting and evaporation) of the target material behind the shock wave front. The duration of the PALS laser pulse is considerably (100–200 times) shorter than the decay time of the crater-producing shock wave. Therefore, the crater volume is determined with a high accuracy by the energy transferred to the material behind the shock wave front during the laser pulse.

The laser-produced plasma state and ablation pressure value are determined by three effects, namely by fast-electron

https://doi.org/10.1017/S0263034615000452 Published online by Cambridge University Press

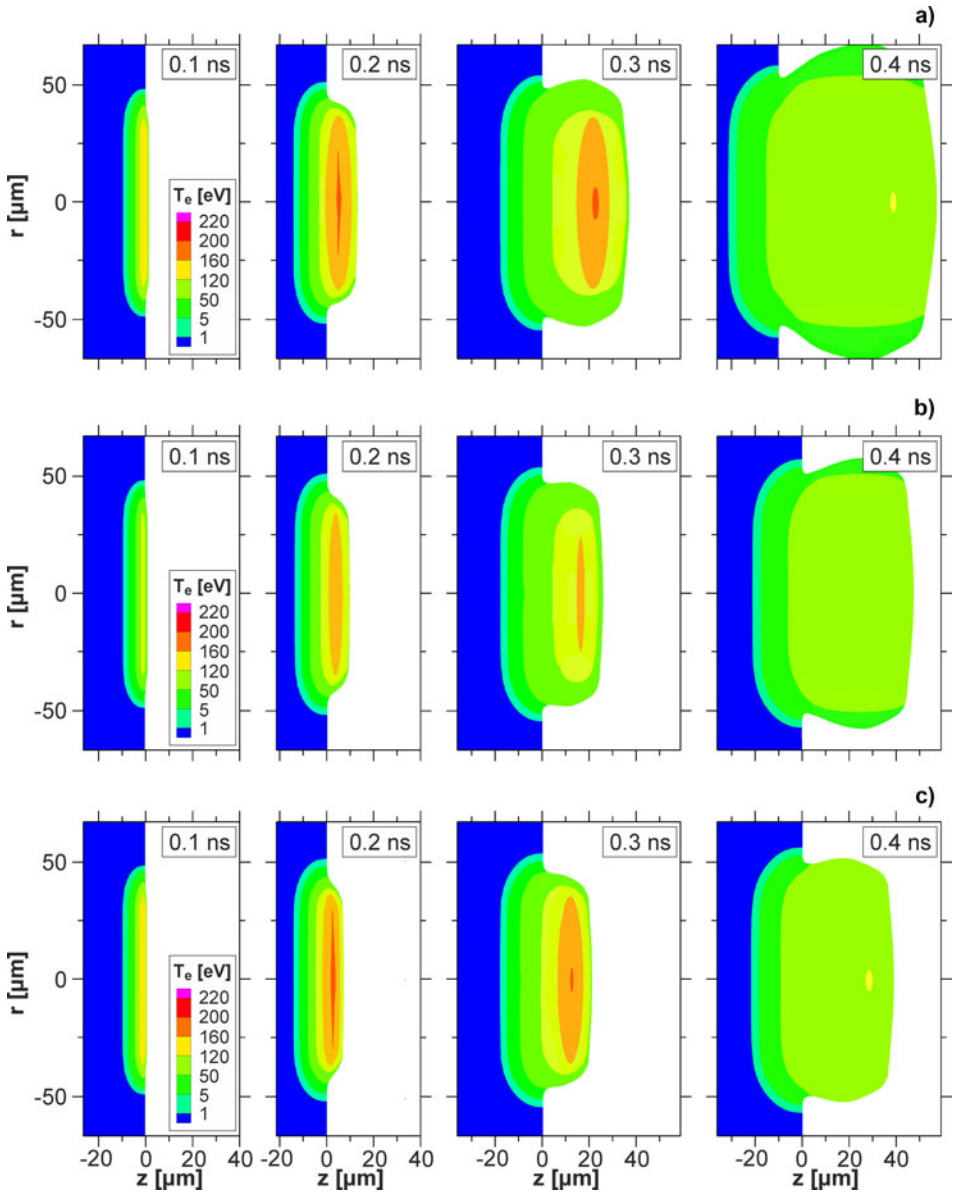

Fig. 8. Spatial distribution sequences of the plasma electron temperature during the laser pulse action for different ablators: a – Cu, b – Ag, and c – Ta.

energy transport, thermal electron conductivity, and lateral plasma expansion.

Assuming a value of the coupling parameter $I\lambda^2$ smaller than 10^{14} Wμm^2/cm^2, the collisional absorption dominates. This bears upon the higher efficiency of the inverse-bremsstrahlung absorption for the third harmonic of the laser radiation, as the critical surface is located closer to the target surface. This results in enhanced attenuation of the laser radiation reaching the critical surface. Besides, the plasma temperature decreases with the increasing beam radius and thus the inverse-bremsstrahlung absorption efficiency grows. Intentionally, the experimental conditions of the target irradiation were chosen to reduce the coupling parameter value below the value stated above, namely to $I\lambda^2 = 3.5 \times 10^{13}$ W μm^2/cm^2. Under these conditions the resonance absorption and consequently also the role of fast electrons are irrelevant (Gus'kov *et al.*, 2014). Therefore only the two other factors should be taken into consideration.

The thermal electron conductivity plays an important role. The transfer of the laser energy to the ablation surface consists of two stages: (i) The laser energy deposition at the critical electron density area and (ii) transport of the deposited energy to the ablation surface. The efficiency of the latter process depends on a composition and state of the plasma. While in the case of light ablators (CH and Al) the ablative plasma can easily reach higher temperatures, this effect cannot occur in the case of heavy ablators due to the plasma radiative cooling. Here we point out a quantitative convergence of the Al plasma temperatures obtained experimentally and numerically in all cases of the ablators used.

https://doi.org/10.1017/S0263034615000452 Published online by Cambridge University Press

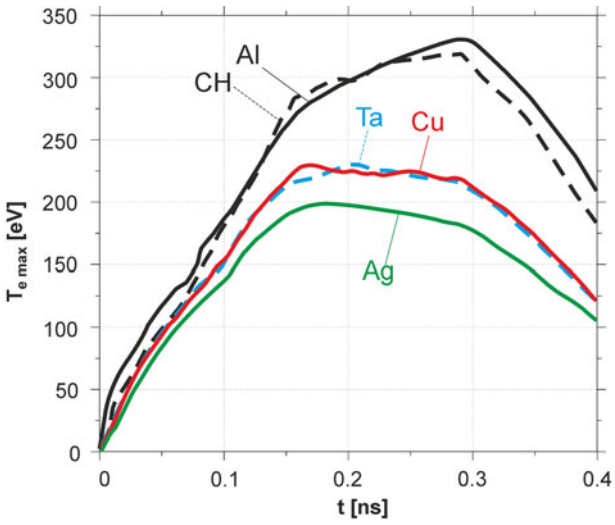

Fig. 9. Temporal profiles of the maximal electron temperature of the Al plasma in the period of the laser action depicted for different ablators.

The large plasma temperatures attainable with light ablators suggest that the ablative plasma pressure can create, via the shock wave action, the crater volumes larger than those corresponding to heavy ablators. However, these crater volumes, especially in the case of the CH ablator, turn out to be smaller when compared with the others. To explain this contradiction, the lateral plasma expansion, which also influences the laser-produced plasma state and the ablation pressure value, should be considered. For this purpose, the spatial distribution of the plasma temperature demonstrated for different ablators in Figures 7 and 8 prove to be useful. As seen in these figures, the temperature spatial distributions inform also about the plasma expansion geometries: The light plasmas expand rather hemispherically, while the heavy ones axially. Such essential difference in the plasma expansion geometries seems to be the main reason of differences in the crater volumes.

Based on these considerations we can formulate the final conclusion that the low-energy loss due to the plasma self-radiation leads to the 2D (hemispherical) geometry of the plasma expansion, which in turn reduces the efficiency of the ablative plasma energy transfer into the target. The design of the ICF pellets should take into account not only the radiative cooling of the ablative plasma, but also the efficiency of the laser energy transport to the inner pellet components.

ACKNOWLEDGMENTS

This work was supported in part by the Access to Research Infrastructure activity in the 7th Framework Program of the EU Contract No. 284464, Laserlab Europe III, by the Czech Republic's Ministry of Education, Youth and Sports under PALS RI project (LM2010014), by National Centre for Science (NCN), Poland under Grant No. 2012/04/M/ST2/00452, and by the ToIFE project of the EUROfusion Consortium. The participation of O. Renner and M. Smid was supported by the ASCR Project No. M100101208.

REFERENCES

Gus'kov, S.Yu. (2013). Fast ignition of inertial confinement fusion targets. *ISSN* 1063-780*X*, *Plasma Phys. Rep.* **39**, 3.

Gus'kov, S.Yu., Demchenko, N.N., Kasperczuk, A., Pisarczyk, T., Kalinowska, Z., Chodukowski, T., Renner, O., Smid, M., Krousky, E., Pfeifer, M., Skala, J., Ullschmied, J. & Pisarczyk, P. (2014). Laser-driven ablation through fast electrons in PALS experiment at the laser radiation intensity of 1–50 PW/cm^2. *Laser Part. Beams* **32**, 177.

Gus'kov, S.Yu., Rozanov, V.B. & Rumyantseva, M.A. (1997). Equations of state for metals (Al, Fe, Cu, Pb), polyethylene, carbon, and boron nitride as applied to problems of dynamical compression. *J. Russ. Laser Res.* **18**, 311. (in Russian).

Jach, K., Morka, A., Mroczkowski, M., Panowicz, R., Sarzyński, A., Stępniewski, W., Świerczyński, R. & Tyl, J. (2001) *Computer Modelling of Dynamic Interaction of Bodies by Free Particle Method*. PWN, Warsaw (in Polish).

Kasperczuk, A., Pisarczyk, T., Chodukowski, T., Kalinowska, Z., Gus'kov, S.Yu., Demchenko, N.N., Ullschmied, J., Krousky, E., Pfeifer, M., Rohlena, K., Skala, J., Klir, D., Kravarik, J., Kubes, P., Cikhardt, J., Rezac, K. & Pisarczyk, P. (2013). Plastic plasma interaction with plasmas with growing atomic number. *Cent. Eur. J. Phys.* **11**, 575.

Kasperczuk, A., Pisarczyk, T., Chodukowski, T., Kalinowska, Z., Gus'kov, S.Yu., Demchenko, N.N., Ullschmied, J., Krousky, E., Pfeifer, M., Rohlena, K., Skala, J. & Pisarczyk, P. (2014). Interactions of plastic plasma with different atomic number plasmas. *Phys. Scr. T* **161**, 014034.

Kasperczuk, A., Pisarczyk, T., Demchenko, N.N., Gus'kov, S.Yu., Kalal, M., Ullschmied, J., Krousky, E., Masek, K., Pfeifer, M., Rohlena, K., Skala, J. & Pisarczyk, P. (2009). Experimental and theoretical investigations of mechanisms responsible for plasma jets formation at PALS. *Laser Part. Beams* **27**, 415.

Lindl, J. (1995). Development of the indirect drive approach to inertial confinement fusion and the target physics basis for ignition and gain. *Plasma Phys.* **2**, 3933.

MacFarlane, J.J., Golovkin, I.E., Wang, P., Woodruff, P.R. & Pereyra, N.A. (2007). A mlti-dimensional collisional radiative code for generating diagnostic signatures based on hydrodynamics and PIC simulation output. *High Energy Density Phys.* **3**, 181.

Marczak, J., Jach, K., Świerczyński, S. & Strzelec, M. (2010). Numerical modelling of laser matter interaction in the region of "low" laser parameters. *Appl. Phys. A* **100**, 725.

Renner, O., Uschmann, I. & Förster, E. (2004). X-ray spectroscopy of hot dense plasmas. *Laser Part. Beams* **22**, 25.

Ribeyre, X., Schurtz, G., Lafon, M., Galera, S. & Weber, S. (2009). Shock ignition: An alternative scheme for HiPER. *Plasma Phys. Control. Fusion* **51**, 015013.

Šmíd, M., Antonelli, L. & Renner, O. (2013). X-ray spectroscopic characterization of shock-ignition-relevant plasmas. *Acta Polytech.* **53**, 233.

https://doi.org/10.1017/S0263034615000452 Published online by Cambridge University Press